International Forum on Aeroelasticity and Structural Dynamics
IFASD 2022
13-17 June 2022, Madrid, Spain

INTEGRATION OF AEROELASTIC EFFECTS IN PRELIMINARY DESIGN OF PSEUDO-SATELLITE PLATFORMS

Alfonso del Carre[1], Zackary K. Krawczyk[2], and Ryan Paul[2]

[1] Skydweller Aero
Arbea Campus, 28108 Alcobendas, Spain
alfonso.delcarre@skydweller.aero

[2] Oklahoma State University
201 General Academic Building, Stillwater, OK 74078
zackary.krawczyk@okstate.edu
ryan.paul@okstate.edu

Keywords: Aeroelasticity, optimization, HAPS, SHARPy.

Abstract: This paper presents Skydweller's approach to account for static aeroelastic effects related to the wing spar design during the preliminary design stage of a solar-powered, ultra-persistent aircraft. The methodology strongly considers multidisciplinary effects through the use of the Simulation of High-Aspect Ratio Aeroplanes in Python (SHARPy) package. Optimization processes for the structural mass of the spar and the twist distribution of a representative T-Tail, High-Altitude Pseudo Satellite (HAPS) aircraft were created with constraints through the use of the L-BFGS-B algorithm. The constraints enforce the maximum deflection of the wingtip, the maximum bending strain in the spar, spar geometry constraints, and continuous and nonincreasing spar dimensions. The structural mass optimizer resulted in significant mass savings over the initial spar. Up to 60 kg of mass savings were achieved in the various run cases, though it should be noted that the initial spar is intentionally oversized. The twist distribution optimization was conducted on the resulting spar geometry of the mass optimization and resulted in a 9.9% reduction in the induced drag at the cruise condition. Through this exercise, a coding framework for preliminary aeroelastic design tools has been developed that will be employed in future design endeavors to improve the performance of HAPS aircraft.

1 INTRODUCTION

The technical progress over the last two decades in materials science, and power storage and generation solutions have enabled a new kind of vehicle: the High-Altitude Pseudo Satellite (HAPS). These configurations offer a set of capabilities that a few years ago would not have been possible to achieve without deploying conventional satellites at a much greater cost. The extremely efficient unmanned air vehicles being developed by Skydweller are designed with the purpose of achieving flight times of the order of weeks or months at a time. Two of the main difficulties when doing so are the energy management during the solar cycle, and the inherent flexibility of the aircraft structure. This paper deals with the latter, with the intention of merging the multidisciplinary analysis of both in a single work in the near future.

Capturing static aeroelastic effects as early in the design loop as possible enables more efficient and safe designs. Further, the distribution of structural mass and the resulting aerodynamic efficiency in terms of induced drag have a direct effect on what the optimal energy management strategy is for an extreme endurance mission. This paper aims to illustrate Skydweller's ongoing modelling and integration efforts to further the state of the art in terms of HAPS platforms by developing and demonstrating a methodology to optimize the design of the primary wing spar to minimize structural weight with ample consideration given to realistic design loads

and other constraints impacting flexible HAPS platforms.

The paper is organized as follows:

- Section 2 introduces the T-Tail HALE configuration, which will be used as a test case in this work, together with the modifications applied to it to make it physically consistent.
- Section 3 presents the methodology of the proposed mass and aerodynamic optimizations as implemented in the SHARPy environment.
- Section 4 shows outputs from the mass and aerodynamic optimization process applied to two versions of a simple representative HAPS configuration. The first set of example results features all the non-structural weight carried centrally at the location of an assumed fuselage, while the second example carries additional mass at the half-span of the wing, representative of wing pylons holding propulsion and energy storage devices. Finally, results are included whereby additional drag savings are sought by applying geometric twist to the undeflected wing spar for the centrally loaded configuration.
- Section 5 concludes by summarizing the findings from the numerical studies and highlights the future work our team has planned to support conceptual design exercises at Skydweller.

2 THE T-TAIL HALE CONFIGURATION

For the purposes of this paper, a representative T-Tail HALE aircraft configuration will be used to demonstrate the preliminary design methodology. This configuration is referenced extensively in the work by Hesse and Palacios [1, 2]. The geometry of this aircraft can be seen in Figure 1. The configuration has been modified to provide a more useful starting configuration for the aerodynamic and structural optimization processes that are covered in sections 3.4 and 3.5. These changes are tied to creating an initial spar geometry that is 2.5 mm thick, which is intentionally oversized in order to provide a starting point for the optimization processes. Details pertaining to the creation of the new spar are covered in section 4.1.

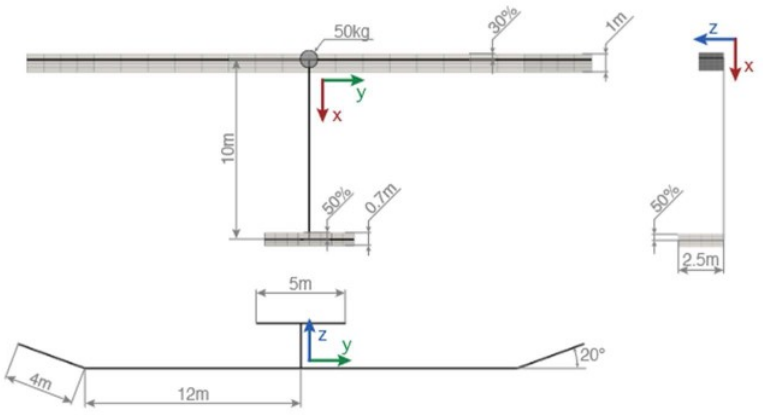

Figure 1: T-Tail HALE Configuration. From [3]

2.1 Spar Geometry for Numerical Studies in this Paper

For demonstration of the methodology presented in this paper, a simplified, hollow rectangular spar geometry with a uniform thickness of 2.5 mm and identical material properties for cap-and-web-components is assumed to be the initial configuration. A depiction of the spar configuration with an exaggerated thickness is shown in Figure 2. In the figure, "E.A." refers to the elastic axis location, located at the center of the beam for the example geometry. While the results reported in this paper utilize the spar configuration described, selection of this geometry is arbitrary and may be modified to different (and more complex) spar designs easily. The initial thickness for our studies was set large knowingly to avoid non-feasible solutions in the early steps of the optimization process. The outer dimensions of the spar geometry, consisting of the height and width, are defined at many spanwise stations, and kept constant throughout the optimization to ensure the feasibility of the solution in the presence of effects such as taper (the spar needs to be contained inside the airfoil cross-section). Over the course of the optimization, the spar thickness, as a function of span, is modified to minimize weight and comply with other constraints, thus improving the aircraft's overall endurance at a constant freestream speed through weight and drag reduction.

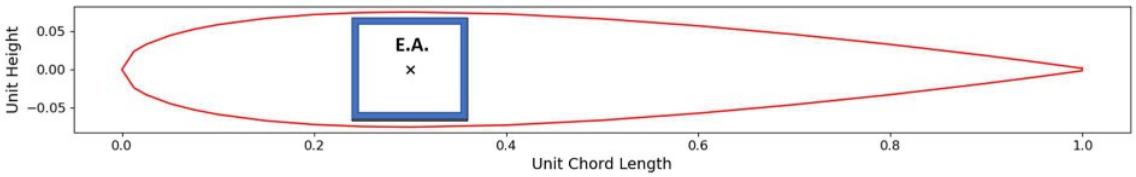

Figure 2: Spar Cross Section

The specific airfoil for the T-Tail HALE model is also not defined in the literature other than the detail that the airfoil features zero camber. For the purposes of sizing the spar, the airfoil is assumed to be a NACA 0015. The primary parameter the optimization modifies, spar thickness along the span, is linked to its mass and structural stiffness. The "non-spar" properties are the corresponding contributions of the other components of the wing, such as the skin and ribs. To keep the thicknesses physically feasible during the optimization, minimum and maximum thicknesses are specified. The maximum thickness is assumed to be the starting thickness of 2.5 mm as it is already known that the initial configuration is oversized. The minimum thickness is assumed to be 0.1 mm as this is on the order of magnitude of a single layer of cured composite prepreg, a likely candidate material for a HAPS wing spar.

As the optimization progresses, bending/torsional stiffness and overall spar weight are continuously updated as the optimizer modifies spanwise thickness seeking minimum spar weight to satisfy the constraints.

3 METHODOLOGY - STRUCTURAL MASS AND AERODYNAMIC OPTIMIZATION APPLIED IN A PRELIMINARY DESIGN CONTEXT

Minimizing structural weight is critical to maximizing the performance of a pseudo-satellite. Inspection of current HAPS prototypes shows that in most cases, their main load bearing element is a single composite material spar. Commonly, existing designs incorporate lightweight ribs, running longitudinally to hold the aerodynamic shape of the wing against air loads, and a very lightweight covering, or solar panels, forming the exterior skin of lifting surfaces in addition to the main spar. As such, the wing spar is responsible for the majority of the bending and torsional stiffness for the wing of HALE aircraft, and accounts for most of the weight of the wing**.**

Our approach to demonstrate structural mass optimization is to focus on the spanwise distribution of material making up the spar. Given an assumed cross sectional spar shape and construction, material properties, and appropriate parameterization, we vary spar geometry with the goal of utilizing all the material making up the spar by achieving a target strain value across the span. Most importantly, we fully capture the associated change in bending and torsional stiffness in specified flight conditions as spar geometry is modified to achieve significant mass savings.

This papers primary contribution comes through development of the *beam_opt* routine in the SHARPy [4] environment, a coupled nonlinear structural and aerodynamic solver. The formulation of this optimization process accounts for multidisciplinary effects as the structural properties and the aerodynamics of the aircraft are connected. This is critically important to capture when designing HALE aircraft, as the wings are oftentimes very flexible and have large wingtip deflections even under a 1g flight load. The use of the medium-fidelity structural and aerodynamic solver, validated by efforts such as Ref. [5], enables static aeroelastic effects to be considered early-on in the design process in a methodology that captures the highly coupled effects of stiffness distribution, overall structural mass, and the effects of beam deflection on span load and the resultant induced drag.

3.1 Goal of Structural Optimization Approach

Several spar optimization processes have been presented in Refs. [6-8] with the goal of weight minimization, but multidisciplinary considerations such as structural load, spanwise deflection, and aerodynamic drag variations as spanwise structural stiffness is modified are not accounted for. The most comparable work to an optimization process that minimizes the mass of a spar is described in Ref. [9] where the optimization of spars for wind turbines was outlined. The approach described in Ref. [9] is a single objective optimization methodology, with spar mass penalized in the cost function, that has several constraints. Similarly, four

constraints were identified for this exercise. These four constraints are:

1) Maximum Bending Strain
2) Maximum Wing Deflection
3) Minimum and Maximum Spar Geometry
4) Continuous Non-Increasing Spar Geometry

As previously stated, the mass optimization exercise will vary the thickness of the spar along the span. For simplification, maximum bending strain was selected as the first constraint, as opposed to a maximum strain that includes other sources of stress such as torsion. This was done, as the main parameter of the model that will be affected by a thickness change is the bending moment stiffness EI_y, which can be expressed as:

$$EI_y = E\left[\frac{bh^3}{12} - \frac{(b-2t)(h-2t)^3}{12}\right] + EI_{y\,non-spar} \quad \text{Eq. 1}$$

The effect of thickness is not as steep for the torsional stiffness, GJ:

$$GJ = G\left[\frac{2t(bh)^2}{(b+h)}\right] + GJ_{non-spar} \quad \text{Eq. 2}$$

Spar mass per unit length ($\bar{m}$) will also be updated with a change in thickness. $\bar{m}$ is expressed as:

$$\bar{m} = \rho(bh - (b-2t)(h-2t)) + \bar{m}_{non-spar} \quad \text{Eq. 3}$$

Bending strain (ε) is defined as follows:

$$\varepsilon = \frac{My}{EI_y} \quad \text{Eq. 4}$$

Due to the geometry, y will be the maximum height of the spar from the elastic axis, as the largest bending strain will always result at the furthest distance from the elastic axis. For a given loading condition, strain will increase as the mass of the structure is reduced. This is due to the decrease in area of the structure which thereby decreases I_y. Naturally, as I_y is reduced, bending strain is increased.

To avoid bending strain becoming too large due to the goal of the mass optimization, the first constraint is enforced and any spar geometry candidates that exceed the maximum bending strain along the main spar are disallowed. The maximum bending strain, as used in the constraint, is calculated using the material's yield stress (σ_{yield}), modulus of elasticity (E), and an appropriate margin of safety (n):

$$\varepsilon_{max} = \frac{\sigma_{yield}}{En} \quad \text{Eq. 5}$$

By evaluating the strain at each structural node (described later in Section 3.3.1) at the maximum loading condition using Eq. 4 and comparing each value to the maximum bending strain value from Eq. 5, the first constraint can be enforced. The max loading condition for traditional aircraft may be set by static load requirements or, more commonly, by instantaneous dynamic loads imposed by gust encounters or turbulence. HAPS design guidance and certification requirements are not well-defined, and applying standard certification bases such as CS-23 that rely on empirical data and accumulated knowledge on conventional aircraft results in sub-optimal, and sometimes non-conservative modelling. The existing certification bases can be made suitable for these aircraft through tailoring until a specific norm is released. The structural flexibility makes traditional static load threshold requirements impractical to assume, and traditional methods for evaluating gust loads are not applicable, necessitating approaches such as that in Refs [10, 11]. An optimum wing spar will approach the condition that spanwise strain approaches ε_{max} at the max loading expected during mission performance. For this exercise, a maximum loading condition of a static 2g trimmed flight condition has been chosen as an aggressive but not unrealistic load factor for this kind of aircraft, given the reduced control authority and

limited envelope. It shall be noted that this is a design decision for this sample case only, and the constraint can be easily modified without impacting the formulation of our methodology.

The second constraint is the maximum wing deflection measured at the wingtip. Due to the extreme aspect ratios of HAPS aircraft, the wing deflections that result from changing the structural stiffness can become large and impractical before the maximum strain is achieved. By specifying a maximum allowable wing deflection, this scenario is avoided. Our current results check deflections only at the wingtip, however additional spanwise constraints could be added.

The final two constraints are enforced to make the spar configuration practical from a manufacturing perspective. The minimum and maximum spar geometry constraint is imposed by specifying bounds on the thickness. This constraint is a byproduct of the already established minimum and maximum thicknesses that are assumed to be .1 mm and 2.5 mm respectively. This effectively limits the design space from going into thicknesses that are impractical and avoids physically impossible solutions such as negative thickness values which are mathematically viable. This constraint is also useful as there is a physical limit to the minimum spar thickness that can be achieved through aerospace manufacturing processes. Lastly, discontinuous spar geometry cannot be replicated in the real world and have no value to this analysis. To produce geometries that are useful, the spar will only be allowed to decrease in thickness along the span and discontinuities will be removed. This constraint is done in post-processing and is not actually enforced during the mass optimization iterative steps.

3.2 Goal of the Aerodynamic Optimization

Beyond mass optimization, minimizing the required cruise power is also imperative in increasing the endurance of pseudo-satellites. This is achieved by maximizing the aerodynamic efficiency,

$$\mathrm{E} = \frac{L}{D} \qquad \text{Eq. 6}$$

Broadly speaking, this has traditionally been achieved by assuming a planar wing and enforcing an elliptical lift distribution at cruise and increasing the aspect ratio as much as possible. Prandtl's elliptical lift distribution results from several assumptions, such as a planar wing, that do not hold necessarily true for HAPS airframes. Furthermore, it is optimal from a purely aerodynamic point of view, not accounting for its structural mass impact. While commercial aircraft are usually constrained in terms of span dimensions, HAPS aircraft have a constraint in minimum wing surface area to complete mission requirements based on expected exposure to solar radiation, which relates directly to generated power.

For the purposes of this paper, the twist distribution of the spar will be optimized in a separate aerodynamic optimization process to minimize the required cruise power, P, defined simply as:

$$\mathrm{P} = \mathrm{T} \cdot \mathrm{V}_{\infty} \qquad \text{Eq. 7}$$

with T being the required thrust force for 1g level flight.

During the aerodynamic optimization, the structural stiffness and mass values will be reused from a previous mass optimization run. The thrust required for steady, level cruise flight is taken to be equal to the amount of induced drag when the aircraft is trimmed. This decision is an artifact of using an inviscid aerodynamic solver. The current work does not consider airfoil profile drag or other forms of drag (such as fuselage or intersection contributions), but rather intends to demonstrate the feasibility and performance of the algorithm. Using SHARPy, a multidisciplinary solution to the aerodynamic optimization is achieved. By varying the twist along the span, the loading of the wing is altered. Due to the structural coupling, the effects on the associated change in wingtip deflection and strain are captured. This can provide additional mass savings in the future.

3.3 SHARPy Overview

SHARPy is a nonlinear analysis package intended for the study of coupled structural and aerodynamic models. This tool is invaluable for the evaluation of highly flexible HALE and HAPS aircraft, as most traditional aircraft analysis methods assume that the structure is rigid, or stiff enough to justify linear assumptions. Using the coupled structural and aerodynamic modules in SHARPy, the optimization routines can be conducted

capturing effects that are traditionally reserved for much later in the design process. The relevant SHARPy modules and processes used in optimization routines will now be defined.

3.3.1 SHARPy Structural Model

The structures in SHARPy are represented by a Geometrically-Exact Composite Beam model based on the works from Géradin & Cardona [12] and Hesse, Palacios, & Murua [2]. Effectively, each major structural component of an aircraft (wings, tail, fuselage, etc.) is consolidated into a slender 1-D beam that aligns with the elastic axis. Each beam is made up of several nodes. Nodes are the most fundamental structural component as these are simply three-dimensional coordinates that define the elastic axis location. Given a loading condition, the deflections and rotations of these nodes are calculated using the SHARPy structural solver. An example of the nodal discretization of the X-HALE aircraft [13] can be seen below in Figure 3. In the sample geometry, more nodes are located along the wing in order to increase the fidelity of this portion of the model while less nodes are concentrated along structures that are under less load in-flight, such as the horizontal and vertical tail surfaces. This example demonstrates the flexibility of the SHARPy analysis package and its ability to handle complex geometries.

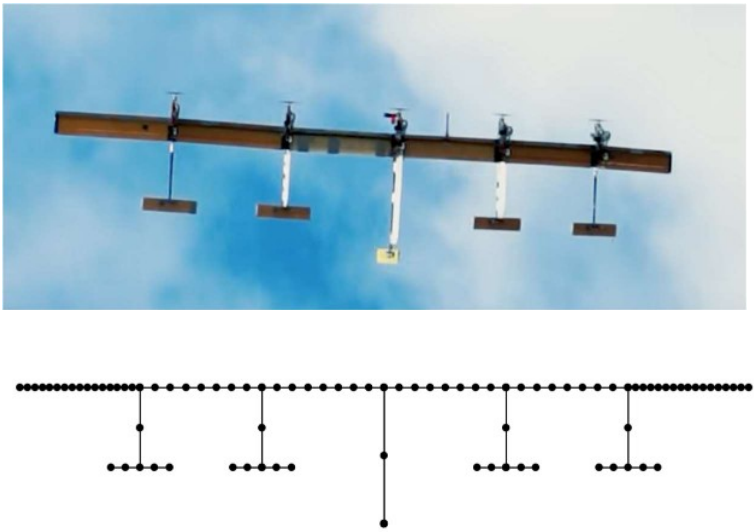

Figure 3: Example of the X-HALE Structural Model Node Discretization in SHARPy

An element consists of three nodes and defines the associated stiffness and mass properties of the nodes contained in it. When discretizing geometries into SHARPy input files, an aircraft is typically first broken up into sections and then each section is defined with several elements. A visual representation of elements and nodes can be seen in Figure 4. Consider this to be a full wing section. As can be seen, the wing section is defined using a total of 5 nodes and 2 elements. By increasing the number of elements and nodes, the fidelity of the model can be adjusted accordingly to represent the wing section's structural properties and behavior more accurately. It should also be noted that the nodes do not have to be equally spaced, giving further flexibility in discretizing the model.

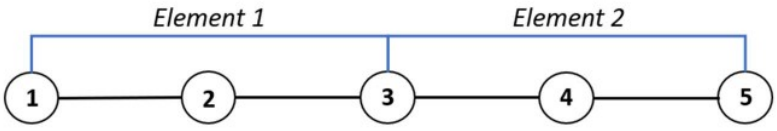

Figure 4: Node and Element Representation

Each element has an associated stiffness and mass matrix. The stiffness matrix can be seen in Eq. 8. The first three values along the diagonal are the structure's resistance to length deformations in the corresponding three-axis local material reference frame, while the last three values are associated with the resistance to the corresponding angle of twist in the local material reference frame. The values themselves are dependent on the material properties (E and G) and the geometric properties (A, J, I) of the structure**.**

$$K = \begin{bmatrix} \mathrm{EA}_x & & & & & \\ & \mathrm{GA}_y & & & & \\ & & \mathrm{GA}_z & & & \\ & & & \mathrm{GJ} & & \\ & & & & \mathrm{EI}_y & \\ & & & & & \mathrm{EI}_z \end{bmatrix} \quad \text{Eq. 8}$$

The local material reference frame that defines the corresponding properties in Eq. 8 is depicted in Figure 5 as reference frame B and is defined at each node. The orientation of the reference frame is associated with the beam as the x-direction is always tangent to the beam in the increasing node direction. The y and z directions are defined using a frame of reference delta vector as in NASTRAN, but generally the z direction is up and the y direction is oriented so that the reference frame is right-handed. Further elaboration on how reference frame B is defined can be found in the work by one of the authors [3]. Reference frame A is the body-fixed frame that allows tracking of the rigid body dynamics. All reference frame positions and orientations are tracked relative to the inertial frame, denoted as frame G in the figure.

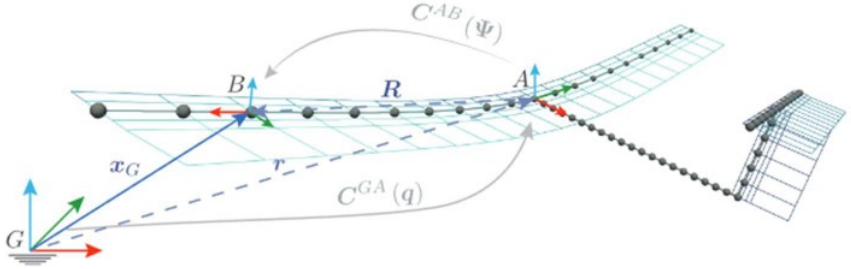

Figure 5: Frames of Reference for SHARPy Structural Solver [10]

The mass matrix, Eq. 9, consists of four 3x3 submatrices:

$$\begin{bmatrix} \bar{\mathrm{m}}\mathrm{I}_3 & -\tilde{\xi}_{\mathrm{cg}}\bar{\mathrm{m}} \\ \tilde{\xi}_{\mathrm{cg}}\bar{\mathrm{m}} & \mathrm{I}_{\mathrm{m}} \end{bmatrix} \quad \text{Eq. 9}$$

The upper left matrix ($\bar{\mathrm{m}}\mathrm{I}_3$) is simply an identity matrix with each value being the mass per unit span of the element. The lower right matrix (I_{m}) is the full mass moment of inertia tensor of the element. Lastly, the two off-diagonal submatrices consist of the mass per unit length value ($\bar{\mathrm{m}}$) multiplied with the beam cross-sectional center of gravity location vector (ξ_{cg}) defined with respect to the elastic axis. This value should not be confused with the overall center of gravity location of the aircraft. The ξ_{cg} vector location is the center of gravity location due to the local distribution of mass associated with the element. These ξ_{cg} and $\bar{\mathrm{m}}$ values are then put through the skew symmetric matrix operation ($\tilde{\bullet}$), yielding the following matrix,

$$\tilde{\xi}_{\mathrm{cg}}\bar{\mathrm{m}} = \begin{bmatrix} 0 & -\xi_{\mathrm{z}}\bar{\mathrm{m}} & \xi_{\mathrm{y}}\bar{\mathrm{m}} \\ \xi_{\mathrm{z}}\bar{\mathrm{m}} & 0 & -\xi_{\mathrm{x}}\bar{\mathrm{m}} \\ -\xi_{\mathrm{y}}\bar{\mathrm{m}} & \xi_{\mathrm{x}}\bar{\mathrm{m}} & 0 \end{bmatrix} \quad \text{Eq. 10}$$

to create the full 3x3 matrix. This center of gravity location vector is given in the material frame of reference.

Additionally, other structural conditions can be added to specific nodes or elements. Non-zero structural twists can be applied to any element – these are in reference to the beam geometry in an un-loaded condition. Also, follower applied forces and moments can be specified at any node to model thrust and the associated angular momentum from a propeller, for example. Similarly, lumped masses can be applied to any node to represent additional loading conditions on the structure such as nacelles or landing gear. Lumped masses can also be given an inertia. The inputs to the SHARPy structural model used in this paper have now been defined. A summary of these inputs can be found below in Table 1.

Table 1: SHARPy Structural Input Summary

Input Description	Type
Nodal 3-D Coordinate Locations	Nodal
Material Properties (E and G)	Stiffness Matrix
Beam Geometric Properties (A, J, I)	Stiffness Matrix
Mass Per Length ($\bar{m}$)	Mass Matrix
Mass Moment of Inertia	Mass Matrix
Center of Gravity Location from Elastic Axis (ξ)	Mass Matrix
Structural Twist	Element
Applied Forces	Nodal
Lumped Mass	Nodal
Lumped Mass Inertia	Nodal
Lumped Mass Position	Nodal

3.3.2 SHARPy Aerodynamic Model

For aerodynamic force calculations SHARPy utilizes an unsteady vortex lattice method (UVLM) [14] with a non-conventional force evaluation scheme defined by Simpson, Palacios, and Murua [15] that is able to handle large sideslip angles. The UVLM is an efficient computational technique to solve 3-D potential-flow problems about moving (and deforming) lifting surfaces. Additionally, a quasi-steady implementation of a vortex lattice method is supported, as is utilized herein for trim calculations during straight and level flight conditions.

SHARPy models the aerodynamics of lifting surfaces, including interaction between lifting surfaces. In SHARPy, at least two continuous nodes are required to form an aerodynamic surface. Each aerodynamic surface is given a chord distribution, twist distribution, airfoil distribution (to handle linear transformations between two airfoils), and elastic axis location with respect to the lifting surface to handle transference of aerodynamic force to structural nodes. The chord, twist, elastic axis, and airfoil distributions are defined at every node to achieve various geometries such as taper. Additionally, each aerodynamic surface must also be given a chordwise paneling input. This specifies the number vertical panels that form the aerodynamic grid. The number of spanwise panels does not have to be specified, as this is defined by the nodal locations. Control surfaces can also be added by specifying a location, chord length, and deflection angle. The location of the control surface is defined as a starting and ending node location, while the chord length and deflection angle are self-explanatory. By defining all these inputs, aerodynamic forces can be calculated and used in the many different analysis modules in SHARPy. Table 2 summarizes the parameters utilized to generate the aerodynamic discretization in the SHARPy environment.

Table 2: SHARPy Aerodynamic Input Summary

Input	Type
Chord Distribution	Nodal
Twist Distribution	Nodal
Airfoil Distribution	Nodal
Elastic Axis Location	Nodal
Chordwise Paneling	Surface
Control Surface Location	Nodal
Control Surface Deflection Angle	Surface
Control Surface Chord	Surface

3.3.3 SHARPy Modules

SHARPy has many analysis modules that can be used for various purposes. For this paper, the module Static Trim will be used to enforce 1g and 2g flight conditions to evaluate the maximum loading and cruise performance of different configurations. Static Trim calls upon a module known as Static Coupled, which in turn calls a structural solver, and an aerodynamic solver module. An overview of these modules will now be given.

The “Static” term in the aerodynamic solvers title simply means that the output has no time dependence through wake convection. All the modules used in this optimization are static, so this is true for their solutions as well. The results in this exercise were all generated with the horseshoe wake modeling option activated, achieving

very relevant speedups. In SHARPy, the Static-UVLM solver calculates the aerodynamic forces and moments given air density, freestream velocity, angle of attack, and the aerodynamic model inputs that have been outlined in the previous section. A summary of the Static-UVLM solver is shown in Figure 6.

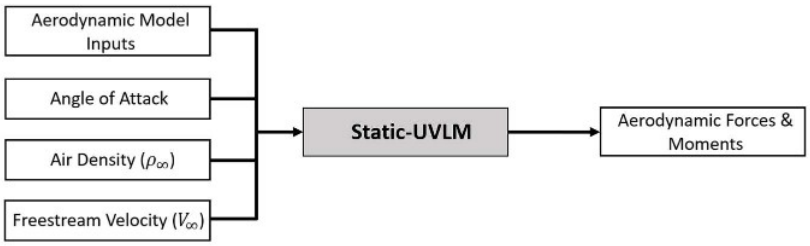

Figure 6: Static-UVLM Summary

The structural solver module, Nonlinear-Static, solves for the nonlinear deflections and rotations of the structural nodes. This is done by inputting the gravity forces and moments of the structure, any external applied forces and moments, and the structural model inputs described above. A summary of the Nonlinear-Static structural solver is shown in Figure 7.

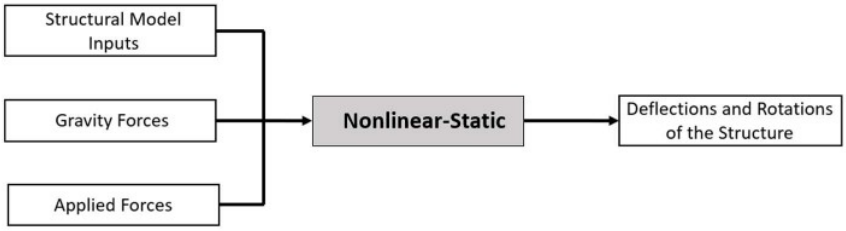

Figure 7: Nonlinear-Static Summary

The overall goal of Static Trim is to find the condition at which the sum of forces and moments experienced by the aircraft are zero with respect to a reference frame level to the ground. This identifies a trimmed, level-flight condition. The module begins by calling the module Static-Coupled (Figure 8) which couples the structural and aerodynamic solvers and finds the coupled static, steady state solution of the configuration. This is achieved by inputting the Static-UVLM force outputs into the Nonlinear-Static module as applied forces. At steady state, all the forces and moments on the aircraft are known for the deformed geometry and current aerodynamic discretization. Based on the net horizontal force, vertical force, and pitching moment determined in sub-iterations to populate a simplified diagonal Jacobian matrix, the Static Trim algorithm updates the angle of attack, thrust, and the elevator deflection angle in a Newton-Raphson type iteration. This is done until the sum of all forces and moments is zero and the aircraft is successfully trimmed to a steady state flight condition. An overview of Static Trim is shown in Figure 9.

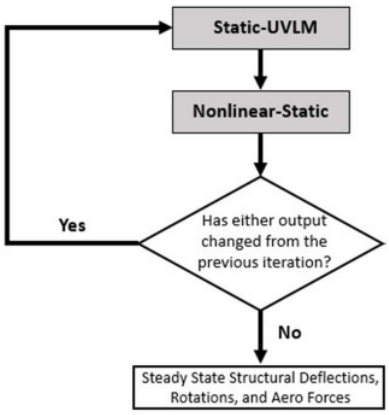

Figure 8: Static Coupled Summary

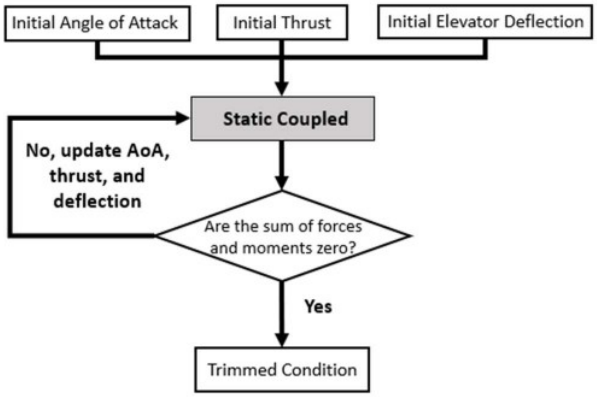

Figure 9: Static Trim Summary

3.4 Mass Optimization Process

With the SHARPy modules defined, the steps of the optimization process will now be elaborated on. This process is intended to begin with an existing preliminary design model where the aerodynamic surfaces and the geometry have been defined, as well as the expected cruise velocity. The design under consideration must be parameterized and stored as a SHARPy input file, incorporating the shape of the lifting surfaces, the initial structural stiffness values, and location of any applied forces or lumped masses to represent the layout of payloads. In general, any lifting surface of the model can be run through this mass optimization procedure, but for this exercise the scope will be limited to the main wings of the aircraft.

The optimization process is conducted in Python using the scipy.optimize package[16]. In this package the minimize function is a minimization algorithm for multivariate scalar functions. The minimization method that is used for all cases is L-BFGS-B [17]. This method is suitable for constrained problems where Hessian information is not easy to generate.

To call the optimization driver, a cost function and an initial guess must be given. For this exercise, the initial guess vector is made of six equally spaced EI_y values that fully define the stiffness of the wing structure starting from the root and ending at the wingtip. Linear interpolation is used to calculate the EI_y values at intermediate locations. Six values have been chosen as a compromise when considering computational time. Bounds can also be placed on the variables input into the minimize function. This limits the design space and speeds up convergence. The bounds on the bending stiffness parameters are implicitly defined through the maximum and minimum thickness constraint and an assumed modulus of elasticity, in the present study.

The return of the function considered by the minimization algorithm is the value that will be minimized. In this instance, the return is the normalized mass of the aircraft configuration with the initial mass based on the 2.5 mm thick spar geometry. Normalization of the mass is conducted to ensure that all quantities involved in the optimization process are of the same order of magnitude. An algorithmic view of the cost function computation follows:

1) Takes in an EI_y distribution (six linearly spaced values from root to wingtip) and updates the SHARPy input files.
2) Run Static Trim at the max 2g loading condition.

   It is imperative that the spar is designed to handle the max loading condition expected. The maximum loading condition for this exercise will be a trimmed 2g flight condition. At this flight condition, the maximum strain and wing deflection constraints will be evaluated during the mass optimization to penalize configurations that violate these constraints.
3) Calculate the shear, moment, and strain at each node.
4) Add penalties if the max wing deflection or strain is exceeded.
5) Return the cost based on normalized mass with added penalties, according to the equation:

$$C = \frac{\text{mass}}{\text{mass}_{\text{init}}} + \sum_{0}^{i} max\left[0, \frac{\text{strain}_i - \text{max\_strain}}{\text{max\_strain}}\right]^2 + max\left[0, \frac{\text{deflect}_{\text{tip}} - \text{max\_deflect}}{\text{max\_deflect}}\right]^2$$

Solutions that exceed the maximum spanwise strain and violate the tip deflection limit are avoided due to the imposed penalty, while the minimum and maximum spar thickness values are upheld through the bounds set by our geometry limits. A summary of the full mass optimization process is shown as Figure 10.

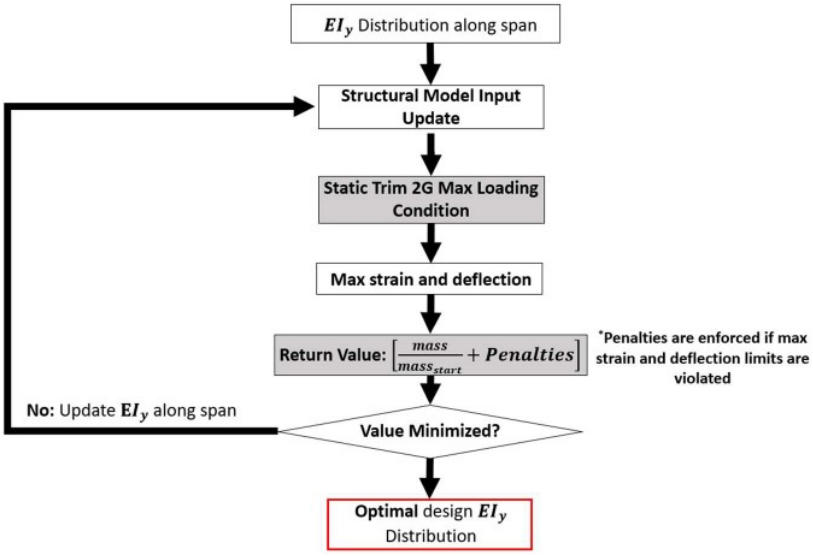

Figure 10: Mass Optimization Process Summary

Using Static Trim in the optimization loop, trimmed flight conditions at the specified cruise velocity are found as the structural stiffness values across the wing are updated. Due to the spar thickness modifying the overall spar weight and resulting aircraft mass, the lift-coefficient of the aircraft at steady cruise varies.

The final constraint, the continuous non-increasing spar geometry, is handled in post-processing, if required. This step is not reflected in Figure 10.

3.5 Aerodynamic Optimization Process

As the optimization in Section 3.4 converges to the lowest spar mass, overall aircraft mass is reduced. Aircraft weight is related to operating aircraft C_L. In the case of steady level flight, $L = W$, thereby reducing aircraft mass reduces operating C_L. This mass reduction has a direct effect on induced drag coefficient, described by the classic lifting line result that shows induced drag coefficient is directly proportional to C_L^2: $C_{D_i} = \frac{C_L^2}{\pi e AR}$, where e represents the span efficiency factor and AR is the aspect ratio for the wing under analysis. In addition to reducing induced drag by lowering the mass of the aircraft, additional drag reduction is sought via geometric twist optimization across the span of the main wing. To find the optimal twist, an additional optimization approach is used as closed form solutions, such as Ref [18], are not applicable due to the coupling between twist, aerodynamic load, and structural deformation for HAPS vehicles.

The aerodynamic optimization is similar to the mass optimization process defined in the previous section. It uses the same scipy.minimize method (L-BFGS-B) and the same constraints to apply penalties to the cost function. Instead of using the normalized mass in the computation of the cost function, the normalized cruise power is returned as the output of the cost function. Finding 1g cruise power requires that the configuration be evaluated through the Static-Trim module at a 1g flight condition in addition to the 2g max loading condition. The max load condition must still be evaluated to ensure that the new twist distribution does not invalidate the optimization constraints such as the max deflection and max strain. For this exercise, the root twist is held constant. Two twist control points will be utilized at the mid-span and wingtip locations whereby twist can be modified during the optimization. Note that the twist values modified by the optimizer are for the spar under jig shape; flight loads result in local twist values along the beam depending on the torsional stiffness and chordwise distribution of the aerodynamic loads applied relative to the elastic axis of the beam. Like the mass optimization process, twist at nodes between the points specified will be calculated using linear interpolation. The steps required for each evaluation of the aerodynamic optimization cost function can be found below:

1. A twist distribution vector, γ, is input into the function and the appropriate aerodynamic SHARPy inputs are updated
2. Static Trim is run using the max 2g loading condition
3. Shear, moment, and strain are calculated at each node using the max loading condition
4. Static Trim is run using the 1g cruise condition.

5. The required power, P, is found from the thrust output from static trim at 1g and Eq. 7
6. Penalties are calculated if the max wing deflection or strain is exceeded
7. Returns the cost function with added penalties, according to the equation:

$$C = \frac{P}{\mathrm{P_{start}}} + \sum_{0}^{i} \max\left[0, \frac{\mathrm{strain}_i - \mathrm{max\_strain}}{\mathrm{max\_strain}}\right]^2 + \max\left[0, \frac{\mathrm{deflect_{tip}} - \mathrm{max\_deflect}}{\mathrm{max\_deflect}}\right]^2$$

The optimizer modifies the γ vector until the minimum required cruise power is found, subject to strain and deflection limits. For the purposes of this paper, this process will be conducted on resulting configurations from the mass optimization process outlined in the previous section. It should be noted that this required power is only the amount that is needed to overcome the inviscid drag. Though this assumption drastically decreases the amount of drag that would be expected and exaggerates savings to required power, it is worthwhile to further demonstrate the capabilities of this process. A summary of the aerodynamic optimization process can be found below in Figure 11.

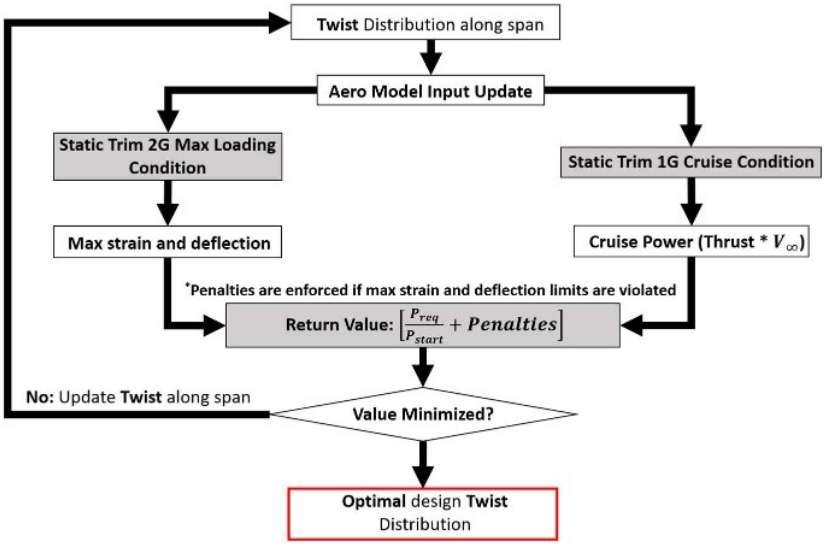

Figure 11: Aerodynamic Optimization Process Summary

4 RESULTS

In the following sections, the results from both the mass and aerodynamic optimizations are presented and elaborated on. First, the spar geometry and corresponding SHARPy inputs of the T-Tail model used for the optimization routines is established and all assumptions are stated. The mass optimization results are then shown for three different run cases:

- Case 1: 0.006 max strain constraint, where geometric constraints (maximum wing tip deflection) are driving the result.
- Case 2: 0.002 max strain constraint, where the max strain, together with the minimum thickness define the solution.
- Case 3: A mass optimization case where additional lumped masses placed at the midspan of the main wing. The additional lumped mass case shows that the optimization processes are robust and can operate on a configuration with mass arbitrarily distributed, rather than being limited to vehicles that carry all their non-structural mass in a centrally located fuselage (and thus limiting most of the optimization to the wing root).

Significant mass savings were achieved over the initial 2.5 mm thick spar in all cases while enforcing the four optimization constraints. Next, aerodynamic twist optimization results are presented using the thickness distribution obtained from the .002 max strain test case to define the spanwise bending and torsional stiffness. Through this optimization, required cruise power due to induced drag was reduced further by 9.9%.

4.1 Modeling the T-Tail Spar Geometry

The base and height of the spar can be seen in Table 3. The height of the spar was made as tall as possible to

maximize the wing's ability to resist bending moment by maximizing I_y for the given geometry, as this will allow for the most mass savings. This geometry was generated using a script that maximized the height given the width, elastic axis location of the spar, and an airfoil. Note that the spar is centered at the 30% chord location which is consistent with the elastic axis location in the SHARPy input files for the previous work featuring the T-Tail HALE. The maximum height was then multiplied by a factor of .9 to ensure that the spar fits within the bounds of the airfoil after accounting for installation constraints. A graphical representation of the spar with the appropriate tolerance factor of .9 and an exaggerated thickness can be seen in Figure 12.

Table 3: Initial Spar Geometry Dimensions

Base of Spar (b)	0.12 m
Height of Spar (h)	0.132 m
Initial Thickness	2.5 mm

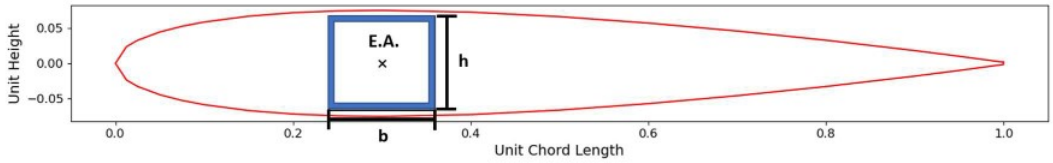

Figure 12: Graphical Representation of Spar Geometry

With the initial spar geometry defined, the stiffness and mass matrix inputs can be updated. The original stiffness and mass matrix properties for the referenced T-Tail HALE model are shown below in Table 4. To fully define the mass and stiffness matrix of the updated spar geometry, the contributions from the other components of the wing that are not the spar (skin, ribs, etc.) must be assumed. As the spar is the only component of the wing that is being changed, these values can be found by using the values in Table 4. By assuming that the spar is 80% of the torsional and bending stiffness and 50% of the mass, the resulting stiffness and mass values are 3000 Nm^2 for GJ, 6000 Nm^2 for EI_y, and 0.375 kg/m for the mass distribution.

Table 4: Original Stiffness and Mass Matrix Values of Main Wing

Bending Moment Stiffness (EI_y)	3.0E+4 N-m^2
Torsional Stiffness (GJ)	1.5E+4 N-m^2
Mass per Span (m)	0.75 kg/m
Torsional Stiffness Not Including the Spar ($EI_{y\ non-spar}$)	3.0E+3 N-m^2
Bending Moment Stiffness Not Including the Spar ($GJ_{non-spar}$)	6.0E+3 N-m^2
Mass per Span Not Including the Spar ($m_{non-spar}$)	0.375 kg/m

The material of the spar is not specified in the references, so intermediate modulus carbon fiber was assumed. The material properties of intermediate carbon fiber with neat resin can be found in [19]. The overall density was assumed to be a combination of 70% of the carbon fiber density [20] and 30% of the neat resin density. By using the assumed spar material properties, the updated stiffness and mass values are calculated for the 2.5 mm thick hollow rectangle. This is done by utilizing Eq. 1-Eq. 3 and using the various spar parameters that have been defined in this section. The resulting stiffness and mass matrix values are listed in Table 5.

Table 5: 2.5 mm Spar Mass and Stiffness Values

Bending Moment Stiffness (EI_y)	5.32E+5 N-m^2
Torsional Stiffness (GJ)	2.99E+5 N-m^2
Mass per Span ($\bar{m}$)	2.37 kg/m

The final mass distribution of the components of the aircraft with the 2.5 mm thick spar are shown in Table 6. The 50 kg payload mass is a lumped mass that is situated at the elastic axis location at the root of the wing. With the spar geometry defined, the optimization process can now be conducted.

Table 6: Initial T-Tail Mass Distribution

Main Wing	75.9 kg
Fuselage	2 kg
T-Tail	2.2 kg
Payload	50 kg
Total Mass	130.1 kg

4.2 Mass Optimization Results

During the optimization, the thickness of the spar is varied along the span at six different control points that are equally spaced from the root to the wingtip. Linear interpolation is used to calculate intermediate values between the six points. A visual representation of the thickness control point locations on the T-Tail model is shown in Figure 13. Note that the additional five points are known from symmetry and are not independently evaluated. For all optimization cases, the equivalent airspeed is assumed to be 14 m/s and thus, the density of the air is set to 1.225 kg/m^3. The goal of the mass optimization is to achieve a thickness distribution that sets the strain at each node location to be as close to the maximum allowable strain as possible while enforcing the four constraints. In doing this, the mass of the spar will be minimized (given a spar geometry and parametrization).

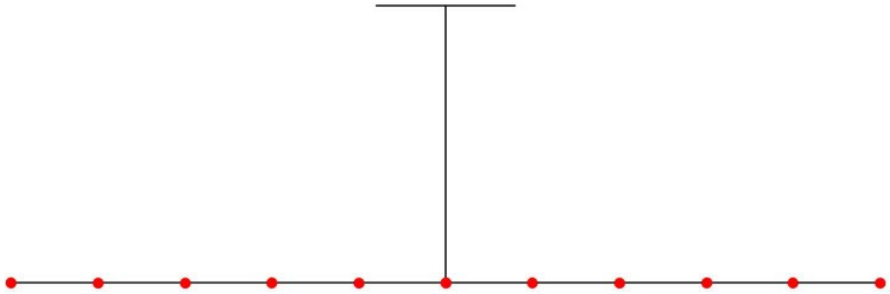

Figure 13: Linear Thickness Control Point Locations for Mass Optimization

To put the results obtained from the subsequent optimization processes into perspective, the performance of the initial 2.5 mm thick spar configuration must be obtained to form a baseline. For this exercise, the focus is on four parameters: the total mass, the cruise power to overcome induced drag at the 1g trim condition at 14 m/s velocity, and the wingtip deflection and the max strain at the 2g max loading condition. These are shown in Table 7. As expected, the maximum strain and wingtip deflection are low as the 2.5 mm thickness results in a stiffer than necessary spar (this would be the case of a primary structure designed for stiffness, and not for strength).

Table 7: Initial 2.5 mm Spar Results

Total Mass (kg)	130.1
Cruise Power (W)	33.9
Wingtip Deflection (m)	1.77
Max Strain	0.00042

4.2.1 Case 1: 0.006 maximum strain constraint

Before beginning the optimization, constraints must be established. By using Eq. 5, the specified yield stress of the intermediate modulus carbon (2453 MPa) [20], and an appropriate margin of safety, the maximum strain was found to be .006. The maximum wingtip deflection was chosen to be 5 m above the unloaded wingtip location. This results in a maximum wingtip deflection of 6.36 m. Though the magnitude of this deflection may be deemed excessive, this was assumed to give the optimizer adequate design space to significantly increase the strain along the span. Lastly, the maximum and minimum thickness values were established in the previous sections.

Table 8: Constraint Values of Case 1 Optimization

Maximum Strain	.006
Maximum Wingtip Deflection (m)	6.36
Maximum Thickness (mm)	2.5
Minimum Thickness (mm)	.1

By running the configuration through the optimization process, significant mass and cruise power savings are achieved. These results can be seen in Table 9. The total mass has been decreased from an initial value of 130.1 kg to 69.9 kg, meaning that the spar is now 60.2 kg lighter along the span. This is due to the significant decrease in the thickness of the spar across the span as shown in Figure 14. The optimizer sets the thickness to a value slightly above the minimum at the root, and by about 3m of span the spar thickness is driven to the minimum allowed by the constraint.

Table 9: Case 1 Optimization Results with a Max Strain of .006 (Case 1)

Total Mass (kg)	69.9
Cruise Power (W)	10.8
Wingtip Deflection (m)	6.35
Max Strain	0.0027

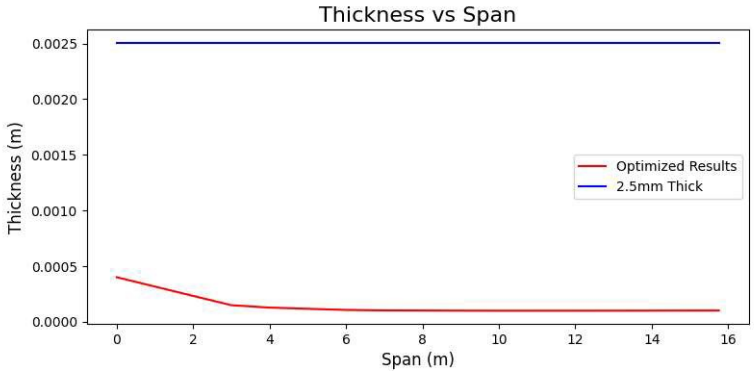

Figure 14: Case 1 Optimization Thickness Results

Based on the results in Table 9 the optimization was limited by the maximum wingtip deflection criteria as opposed to the maximum strain. Figure 18 depicts the wingtip deflection of the optimized result for the .006 maximum strain case and the original configuration. The subsequent strain results of these two configurations be seen in Figure 15. The algorithm is aiming to increase the strain as much as possible at the root but fails to reach the desired .006 maximum strain value due to the wingtip deflection criteria. The strain then decreases significantly around the 6 m span location. This is due to the significant reduction in bending load towards the tip and having reached the minimum thickness constraint. This is shown in Figure 14 where the thickness of the spar is kept at .1 mm from the 6 m span location onwards. This inability to decrease the thickness further results in the corresponding strain decrease.

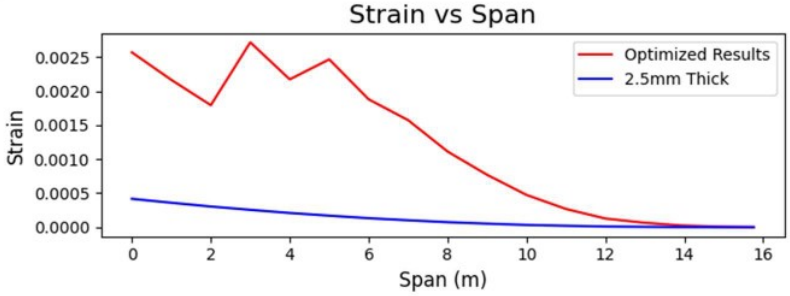

Figure 15: Case 1 Optimization Strain Along the Span

4.2.2 Case 2: 0.002 maximum strain constraint

To evaluate the algorithm's ability to enforce the maximum strain criteria, the maximum strain was lowered to .002 based on the previous results from Case 1. The results from the optimization run with the lower maximum strain can be seen in Table 10 and a comparison of the strain of the two cases can be found in Figure 16. The optimization did an effective job at maximizing the strain toward the root as the maximum strain is approached at several spanwise locations. The strain is once again limited by the minimum thickness constraint beyond the 8 m span location, evidenced by the bending strain as it begins decreasing below the target .002 strain value. This is shown in the thickness results, Figure 17, where the thickness latches onto the lower .1 mm bound of the constraint beyond the 8 m span location.

Table 10: Case 2 Optimization Results with a Max Strain of .002

Total Mass (kg)	70.9
Cruise Power (W)	11.1
Wingtip Deflection (m)	5.17
Max Strain	0.002

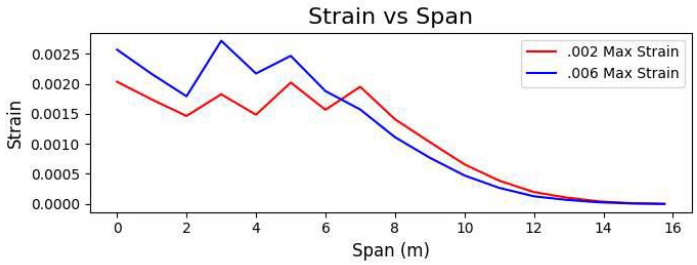

Figure 16: Maximum Strain Result Comparison Between Case 1 (0.006) and Case 2 (0.002)

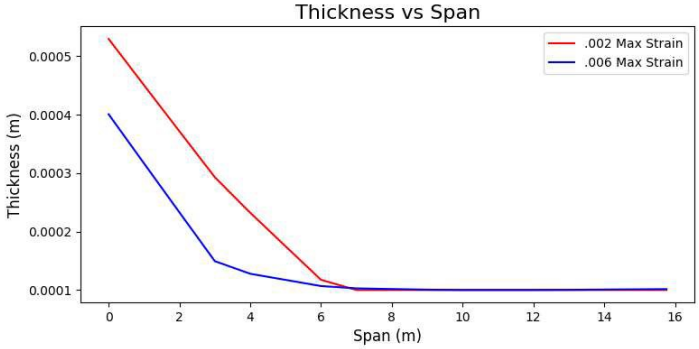

Figure 17: Thickness Result Comparison Between .002 and .006 Max Strain Cases

A comparison of each configuration at the 2g max loading condition can be found below:

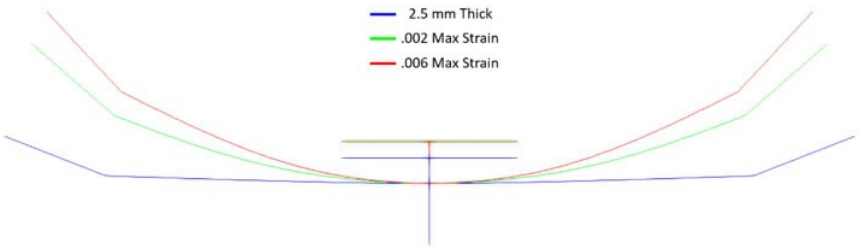

Figure 18: Elastic axis deformation at 2g Max Loading Condition for Baseline, Case 1 and Case 2 results

4.2.3 Robustness Case – Mass Optimization Performance with Additional Lumped Masses at Spanwise Wing Stations

An additional study was performed to investigate the robustness of the proposed approach. In this case, lumped masses were placed at the half-span of each wing, representative of a HAPS configuration with nacelles for the propulsion system and power storage in the wing. A visual representation of the lumped mass locations can be seen in Figure 19. These lumped masses each have a magnitude of 25 kg. An updated mass distribution of the initial 2.5 mm thick spar configuration with the additional lumped masses at the mid-span is shown in Table 11.

Table 11: T-Tail Mass Distribution of 2.5 mm Thick Spar with Additional Mid-Span Lumped Masses

Main Wing	75.9 kg
Fuselage	2 kg
T-Tail	2.2 kg
Payload	50 kg
Each Mid-Span Lumped Mass	25 kg
Total Mass	180.1 kg

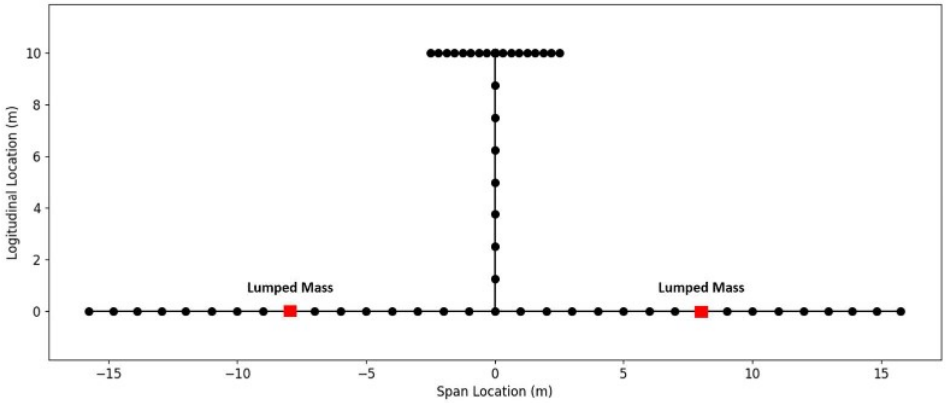

Figure 19: Additional Lumped Mass Locations

A spar was designed for this more complex test case. The presence of the lumped mass can be seen in the bending shear and moment plots shown in Figure 20. The optimization process was then conducted with the same .002 max strain constraint that was used in Case 2 that focused on enforcing the maximum strain constraint.

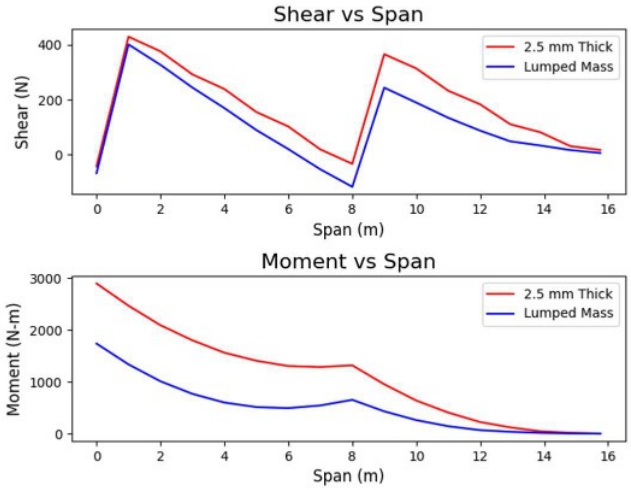

Figure 20: Additional Lumped Mass Shear and Moment Outputs for Original 2.5 mm Thick Spar and Optimized Result (Case 3)

The results of the mass optimization for this case are shown in Table 12. As can be seen, both the wingtip deflection and max strain constraints were encountered. The maximum strain of .0019 is just below the .002

maximum strain constraint while the wingtip deflection of 6.37 m is .01 m above the max deflection constraint. Being over the maximum deflection constraint was deemed acceptable as the magnitude of the difference is rather insignificant. The resulting mass of the configuration without the additional lumped masses is 70.2 kg. This mass result is slightly less than the results obtained from Case 2 (70.9 kg). This is proven by Figure 22 as the thickness distribution for this run case is lower than the .002 max strain result. This is due to the presence of the lumped mass, which caused a discontinuity in the shear (Figure 20) and thus decreased the magnitude of the moment experienced near the root locations.

Table 12: Lumped Mass Optimization Results

Total Mass (kg)	120.2
Total Mass Without Additional Lumped Mass (kg)	70.2
Cruise Power (W)	29.8
Wingtip Deflection (m)	6.37
Max Strain	.0019

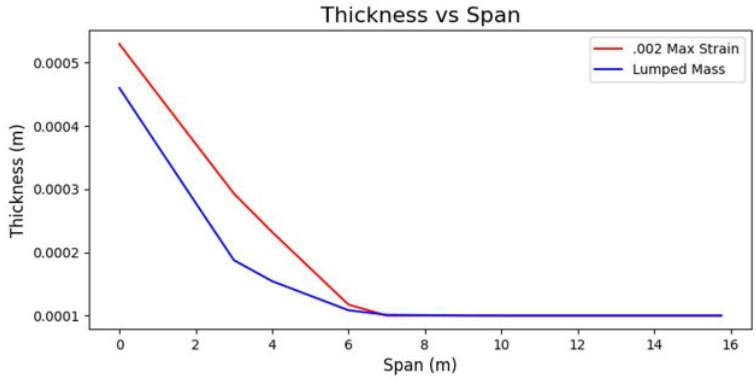

Figure 21: Optimized Thickness Distribution Case 2 and Case 3

The strain results are shown in Figure 22. As shown, the first half of the span was made stiffer to keep the wingtip deflection below the maximum constraint. Evidence of this is provided by the strains being lower than the maximum at these locations. This is a similar trend to what was seen in the strain plots (Figure 15) for Case 1 which was also limited by the maximum wingtip deflection constraint. The lumped mass also creates a local maximum in the bending moment which leads to a larger strain at this location. The algorithm successfully kept the strain at this location below the maximum strain constraint as it only reached a magnitude of .0019. This gives confidence in the optimization algorithm, as it has shown that it has the ability to handle multiple loading conditions while still maintaining the constraints.

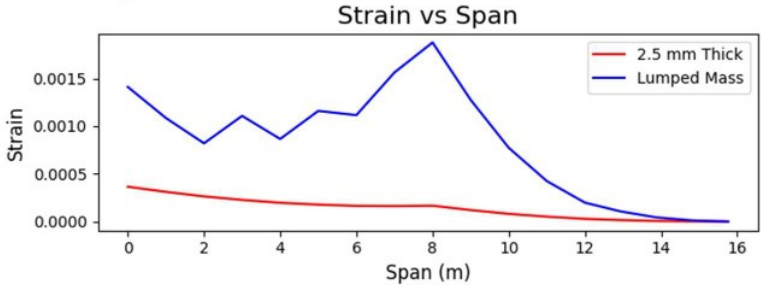

Figure 22: Additional Lumped Mass Strain Output for Original 2.5 mm Spar and Optimized Result (Case 3)

4.3 Aerodynamic Optimization

To further increase the endurance of the HAPS aircraft, the aerodynamic optimization will now be conducted. The location of the linear twist distribution control points is shown in Figure 23. For this exercise, two twist control points at the midspan (t_1) and the wingtip (t_2) will be varied by the optimization process to further decrease the required cruise power. The twist at the root will be left at the initial value of zero. This process is done on the resulting optimized .002 max strain configuration (Case 2). The previous results from the mass optimization on this configuration can be seen in Table 10. These values will be used to evaluate the results of

the aerodynamic optimization output. The thickness distribution from Figure 17 for the .002 max strain case will be used and the thickness will be held constant throughout the process.

The results from the aerodynamic optimization are shown in Table 13. The cruise power was decreased from 11.1 W to 10 W with a linear twist distribution of zero at the root, -0.13˚ at the midspan, and -1.12˚ at the wingtip. In this instance, a positive twist value indicates a leading edge up rotation. This is a 9.9% decrease in required power to overcome induced drag over the untwisted configuration. Of course, adding parasite drag would drastically lower the impact of these results on the actual cruise power savings.

Table 13: Aerodynamic Optimization Results on Case 2 Mass Optimization Configuration

Twist Distribution (°)	[0, -0.13, -1.12]
Cruise Power (W)	10.0
Wingtip Deflection (m)	4.75
Max Strain	.002

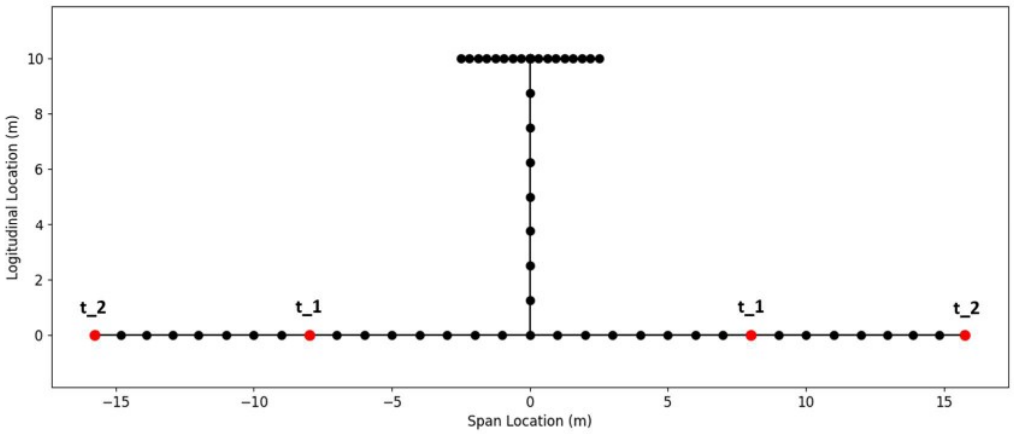

Figure 23: Linear Twist Distribution Control Point Locations

The effect of building a spar with washout in the no-load condition causes unloading of the wingtips, which decreases the wingtip deflection from 5.17 m to 4.75 m. This is due to the subsequent decrease in lift which lowers the shear and moment loads and the strain on the outboard portion of the wing. Note that the maximum strain experienced by the configuration is still .002 as the root strain was not significantly lowered. This trend can be seen below in Figure 24 and Figure 25 which compares the loads and strain between the twisted and untwisted configurations.

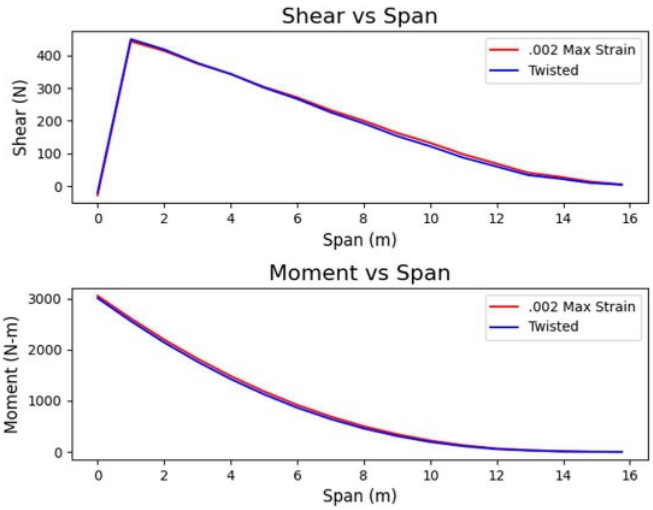

Figure 24: Shear and Moment Plots of Case 2 Mass Optimization and Twisted Configuration

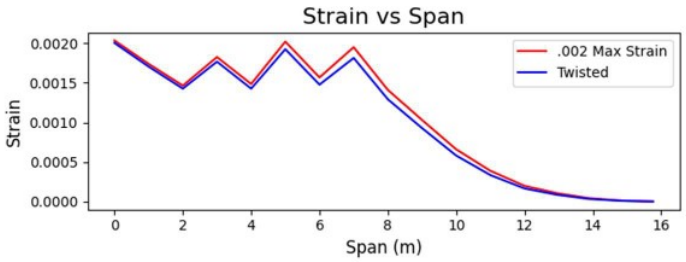

Figure 25: Strain of Case 2 Mass Optimization and Twisted Configuration

5 CONCLUSIONS AND FUTURE WORK

To maximize the endurance of HAPS vehicles, a multidisciplinary preliminary design approach must be employed. This paper successfully demonstrates such a methodology being applied to the spar design of a representative T-Tail HALE configuration. Through this process, a coding framework that utilizes SHARPy has been developed that can be quickly and easily modified to evaluate several HAPS designs. The mass and aerodynamic optimization processes demonstrated in this paper yielded significant mass and cruise power savings while enforcing the stated constraints. This should invoke confidence in the potential of this methodology as this proved true even when the configuration was modified with lumped masses and different limiting constraints were encountered. By enlisting the use of similar types of procedures in the design processes of future HAPS vehicles, a better understanding of the static aeroelastic effects can be found, thus leading to more informed design decisions that lead to improved performance.

The next logical step to improving the methodology that has been presented in this paper is to add viscous drag effects. The limitation of simply relying on inviscid drag calculations in SHARPy is that the associated cruise power is much smaller than what would be anticipated. By including a viscous drag model, the drag savings found throughout the optimization processes would be more indicative of real-world results leading to a more realistic view of the design space and the inherent benefits of design decisions. Additional optimization processes can also be developed that examine other phenomena that are important from a preliminary design perspective. Evaluating the optimum wingspan given a design surface area would be one such example. Oftentimes, the minimum surface area is a design criteria of HAPS vehicles, as the amount of power generation from solar cells is known. This process would naturally pair well with the inclusion of viscous drag. It would also be worth combining the aerodynamic and mass optimization processes that have been presented in this paper. Due to the coupling of the aerodynamic and structural models in SHARPy, treating these processes separately eliminates the potential of further performance improvements. This is evident from the aerodynamic optimization results in Section 4.3. The twist distribution had the effect of slightly unloading the wingtips. This subsequentially lowered the strain at several locations along the span and decreased the wingtip deflection. Though these differences are small and would likely only result in minimal additional mass savings for this model, this cannot be said for other HAPS configurations.

Ongoing work by the authors will deal with the coupling of the two optimization cases here shown, the structural (spar sizing) and aerodynamic (twist distribution). This will result in lift distributions that differ from the classic elliptical distribution, together with lightweight structures explicitly designed for that case.

Another ongoing effort at Skydweller Aero is to couple the in-house solar mission simulator, which has the capability of sizing the battery mass for a given aircraft, mission, and payload, with the aerostructural framework here presented.

6 REFERENCES

[1] H. Hesse and R. Palacios, "Reduced-order aeroelastic models for dynamics of maneuvering flexible aircraft," *AIAA Journal,* vol. 52, no. 8, 2014, doi: 10.2514/1.J052684.

[2] H. Hesse, R. Palacios, and J. Murua, "Consistent structural linearization in flexible aircraft dynamics with large rigid-body motion," *AIAA Journal,* vol. 52, no. 3, 2014, doi: 10.2514/1.J052316.

[3] A. del Carre de la Portilla, "Aeroelasticity of very flexible aircraft at low altitudes," Aeronautics, Imperial College London, Imperial College London, 2020.

[4] A. del Carre, A. Muñoz-Simón, N. Goizueta, and R. Palacios, "SHARPy: A dynamic aeroelastic simulation toolbox for very flexible aircraft and wind turbines," *Journal of Open Source Software,* vol. 4, no. 44, 2019, doi: 10.21105/joss.01885.

[5] R. Palacios, J. Murua, and R. Cook, "Structural and aerodynamic models in nonlinear flight dynamics of very flexible aircraft," *AIAA journal,* pp. 2648-2659, 2010.

[6] C. Kassapoglou, "Simultaneous cost and weight minimization of composite-stiffened panels under compression and shear," *Composites Part A: Applied Science and Manufacturing,* vol. 28, no. 5, 1997, doi: 10.1016/s1359-835x(96)00141-8.

[7] M. Kaufmann, D. Zenkert, and M. Akermo, "Material selection for a curved C-spar based on cost optimization," *Journal of Aircraft,* vol. 48, no. 3, 2011, doi: 10.2514/1.C000188.

[8] C. H. Park, W. I. Lee, W. S. Han, and A. Vautrin, "Simultaneous optimization of composite structures considering mechanical performance and manufacturing cost," *Composite Structures,* vol. 65, no. 1, 2004, doi: 10.1016/j.compstruct.2003.10.010.

[9] J. Zhu, X. Cai, P. Pan, and R. Gu, "Optimization design of spar cap layup for wind turbine blade," *Frontiers of Structural and Civil Engineering,* vol. 6, no. 1, 2012, doi: 10.1007/s11709-012-0147-9.

[10] G. Deskos, A. del Carre, and R. Palacios, "Assessment of low-altitude atmospheric turbulence models for aircraft aeroelasticity," *Journal of Fluids and Structures,* vol. 95, p. 102981, 2020.

[11] J. Murua, R. Palacios, and J. Graham, "Open-loop stability and closed-loop gust alleviation on flexible aircraft including wake modeling," in *53rd AIAA/ASME/ASCE/AHS/ASC Structures, Structural Dynamics and Materials Conference 20th AIAA/ASME/AHS Adaptive Structures Conference 14th AIAA*, 2012, p. 1484.

[12] M. Geradin, Cardona, A., *Flexible multibody dynamics: A finite element approach*. John Wiley, 2001.

[13] A. del Carre, P. Teixeira, R. Palacios, and C. E. Cesnik, "Nonlinear response of a very flexible aircraft under lateral gust," in *International Forum on Aeroelasticity and Structural Dynamics, IFASD, Savannah, Georgia, USA*, 2019.

[14] J. Katz and and A. Plotkin, "Low-Speed Aerodynamics, Second Edition," *Journal of Fluids Engineering,* vol. 126, no. 2, 2004, doi: 10.1115/1.1669432.

[15] R. J. S. Simpson, R. Palacios, and J. Murua, "Induced-drag calculations in the unsteady vortex lattice method," *AIAA Journal,* vol. 51, no. 7, 2013, doi: 10.2514/1.J052136.

[16] "scipy.optimize.minimize." https://docs.scipy.org/doc/scipy/reference/generated/scipy.optimize.minimize.html (accessed May 17, 2022.

[17] C. Zhu, R. H. Byrd, P. Lu, and J. Nocedal, "Algorithm 778: L-BFGS-B: Fortran Subroutines for Large-Scale Bound-Constrained Optimization," *ACM Transactions on Mathematical Software,* vol. 23, no. 4, pp. 550-560, 1997, doi: 10.1145/279232.279236.

[18] A. Gopalarathnam and R. K. Norris, "Ideal lift distributions and flap angles for adaptive wings," *Journal of aircraft,* vol. 46, no. 2, pp. 562-571, 2009.

[19] "Toray BT250E-6." https://www.toraytac.com/media/a2d22600-3f85-4304-8526-2adc73fed148/75526Q/TAC/Documents/Data_sheets/Thermoset/UD%20tapes%20and%20prepregs/BT250E-6_Epoxy_PDS.pdf (accessed May 17, 2022.

[20] "T1100G Intermediate Modulus Carbon Fiber." https://www.toraycma.com/wp-content/uploads/T1100G-Technical-Data-Sheet-1.pdf.pdf (accessed May 17, 2022.